manganese which iodide approaches so as to form (MeCp)Mn $(CO)_3$.

Once (MeCp)Mn(CO)I^- is formed, it may readily pick up one CO to have (MeCp)Mn$(CO)_2I^-$, if only the dissolved CO is available. The methyl cyclopropane from the reaction involving cyclopropylcarbinyl bromide may be assumed to support, in part, this concerted mechanism.

In conclusion, the last two reaction pathways, SET and the concerted pathways may operate in competition in this reaction.

Acknowledgment. Financial support from the Korea Science and Engineering Foundation (92-25-00-04) is greatly appreciated. The authors thank Mrs. M. S. Kim and Mr. D. S. Yun for their preparing this manuscript. Fruitful discussions with Professor G. S. Kim is highly appreciated. Authors also thank the referees for their advice and corrections on this manuscript.

References

1. (a) Kao, S. C.; Spillet, C. T.; Ash, C.; Lusk, R.; Park, Y. K.; Darensbourg, M. Y. *Organometallics* **1985**, *4*, 83. (b) Kao, S. C.; Darensbourg, M. Y. *Organometallics* **1984**, *3*, 646.
2. (a) Arndt, L.; Delord, T.; Darensbourg, M. Y. *J. Am. Chem. Soc.* **1984**, *106*, 456. (b) Slater, S. G.; Lusk, R.; Schumann, B.; Darensbourg, M. Y. *Organometallics* **1982**, *1*, 1662.
3. (a) Nyholm, R. S.; Sabdhu, S. S. *J. Chem. Soc.* **1963**, *92*, 5916. (b) Butler, I. S.; Coville, N. J.; Cozak, D. and *et al. Inorg. Synth.* **1978**, *19*, 188. (c) Zhuang, Jun-Ming; Batchelor, R. J.; Einstein, F. W. B.; Jones, R. H.; Hader, R.; Sutton, D. *Organometallics* **1990**, *9*, 2725. (d) Wieland, S.; Eldik, R. V. *Organometallics* **1991**, *10*, 3110.
4. Kirtley, S. W.; Andrews, M. A.; Bau, R.; Grynkewich, G. W.; Marks, T. J.; Tipton, D. L.; Whittlesey, B. R. *J. Am. Chem. Soc.* **1977**, *99*, 7154.
5. Park, Y. K.; Lee, Y. G.; Kim, G. S. *Bull. Korean Chem. Soc.* (submitted in 1995).
6. (a) Darensbourg, M. Y.; Jimenez, P.; Sackett, J. R.; Hankel, J. M.; Kump, R. L. *J. Am. Chem. Soc.* **1982**, *104*, 1521. (b) Darensbourg, M. Y.; Darensbourg, D. J.; Barros, H. L. C. *Inorg. Chem.* **1978**, *17*, 297.
7. (a) Park, Y. K.; Kim, G. S.; Song, G. O. *Bull. Korean Chem. Soc.* **1995**, *16*, 310. (b) Pou, S. *et al. Anal. Biochem.* **1994**, *217*, 76.
8. (a) Maillard, B.; Forest, D.; Ingold, K. V. *J. Am. Chem. Soc.* **1976**, *98*, 6355. (b) Park, Y. K.; Kim, S. J. *Bull. Korean Chem. Soc.* **1990**, *11*, 109.

Characterization by Solid-State ^{51}V NMRand X-ray Diffraction of Vanadium Oxide Supported on ZrO_2

Jong Rack Sohn*, Man Young Park, and Young Il Pae

**Department of Industrial Chemistry, Engineering College, Kyungpook National University, Taegu 702-701, Korea*

Department of Chemistry, University of Ulsan, Ulsan 680-749, Korea

Received December 26, 1995

Vanadium oxide-zirconia catalysts were prepared by dry impregnation of powdered $Zr(OH)_4$ with aqueous solution of NH_4VO_3. The characterization of prepared catalysts was performed using ^{51}V solid state NMR, XRD, and DSC. The addition of vanadium oxide up to 9 mol% to zirconia shifted the phase transitions of ZrO_2 from amorphous to tetragonal toward higher temperatures due to the interaction between vanadium oxide and zirconia. On the basis of results of XRD and DSC, it is concluded that the content of V_2O_5 monolayer covering most of the available zirconia was 9 mol%. The crystalline V_2O_5 was observed only with the samples containing V_2O_5 content exceeding the formation of complete monolayer (9 mol%) on the surface of ZrO_2.

Introduction

Catalysts based on vanadia supported on various oxides are used in a variety of industrial chemical process. Vanadium oxide catalysts in combination with various promoters are widely used for several reactions including oxidation of hydrocarbons,[1,2] ammoxidation of aromatics and methylaromatics,[3] and selective catalytic reduction of NO_X by NH_3.[4] These systems have also been found to be effective catalysts for the oxidation of methanol to methylformate.[5,6] Much research has been done to understand the nature of active sites, the surface structure of catalysts as well as the role played by the promoter of the supported catalysts, using infrared (IR), X-ray diffraction (XRD), electron spin resonance (E.S.R.) and Raman spectroscopy.[6~9] So far, silica, titania and alumina[10~13] have been commonly employed as the vanadium oxide supports, and comparatively very few works have been reported for zirconia as the support for vanadium oxide.[14~16]

It is well known that the dispersion and the structural features of supported species can strongly depend on the

*To whom all correspondence should be addressed.

support. Structure and other physicochemical properties of supported metal oxides are considered to be in different states compared with bulk metal oxides because of their interaction with the supports. Solid-state nuclear magnetic resonance (NMR) methods represent a novel and promising approach to these systems. Since only the local environment of a nucleus under study is probed by NMR, this method is well suited for the structural analysis of disordered systems such as the two-dimensional surface vanadium oxide phases which is of particular interest in the present study. In addition to the structural information provided by NMR methods, the direct proportionality of the signal intensity to the number of contributing nuclei makes NMR be useful for quantitative studies. In the present investigation, the techniques of solid-state ^{51}V NMR, differential scanning calorimetry (DSC), and XRD have been utilized to characterize a series of V_2O_5 samples supported on ZrO_2 with various vanadia loadings.

Experimental

Catalyst Preparation. Precipitate of $Zr(OH)_4$ was obtained by adding aqueous ammonia slowly into an aqueous solution of zirconium oxychloride at room temperature with stirring until the pH of mother liquor reached about 8. The precipitate thus obtained was washed thoroughly with distilled water until chloride ion was not detected, and was dried at room temperature for 12 h. The dried precipitate was powdered below 100 mesh.

The catalysts containing various vanadium oxide content were preparated by dry impregnation of powdered $Zr(OH)_4$ with aqueous solution of NH_4VO_3 followed by calcining at high temperature for 1.5 h in air. This series of catalysts are denoted by their mol% of V_2O_5. For example, 1-V_2O_5/ZrO_2 represents the catalyst containing 1 mol% V_2O_5.

Characterization. Catalysts were characterized in order to determine the structure of the support as well as that of vanadium oxide by means of a Jeol Model JDX-8030 diffractometer, employing Cu Kα (Ni-filtered) radiation.

^{51}V NMR spectra were measured by a Bruker MSL400 spectrometer with a static magnetic field strength of 9.4 T. Larmor frequency was 105.25 MHz. The ordinary single pulse sequence was used, in which the pulse width was set at 0.8 μs and the repetition time was 0.1 s. The π/2 pulse width adjusted for solution was 12 μs. The spectral width was 1.25 MHz. The number of scans was varied from 1000 to 12000, depending on the concentration of vanadium. The signal acquisition was started at 4 μs after the end of the pulse. The sample was static, and its temparature was ambient (294 K). The spectra were expressed with the signal of $VOCl_3$ being 0 ppm, and the higher frequency shift from the standard was positive. Practically, 0.16 M $NaVO_3$ aqueous solution (−574.28 ppm) was used as the second external reference.[17]

DSC measurements were performed by a PL-STA model 1500H apparatus in air, and the heating rate was 5 K per minute. For each experiment 10-15 mg of sample was used.

Results and Discussion

The crystalline structure of V_2O_5/ZrO_2 calcined in air at different temperatures for 1.5 h was examined. As shown in Figure 1, ZrO_2 was amorphous to X-ray diffraction up

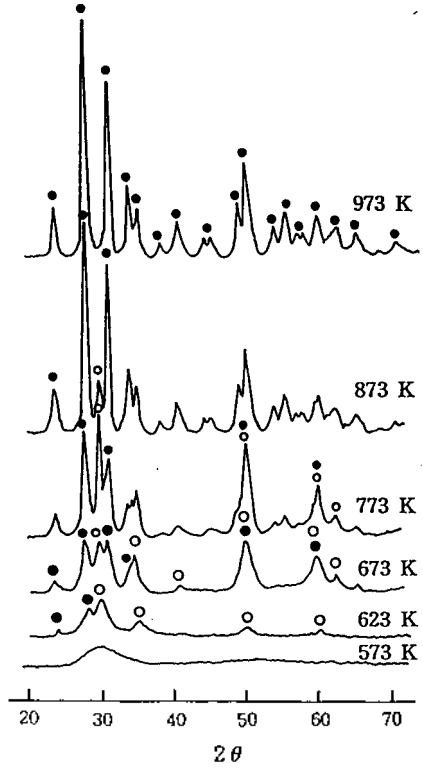

Figure 1. X-ray diffraction patterns of ZrO_2 calcined at different temperature for 1.5 hr. ○ : tetragonal phase ZrO_2, ● : monoclinic phase ZrO_2.

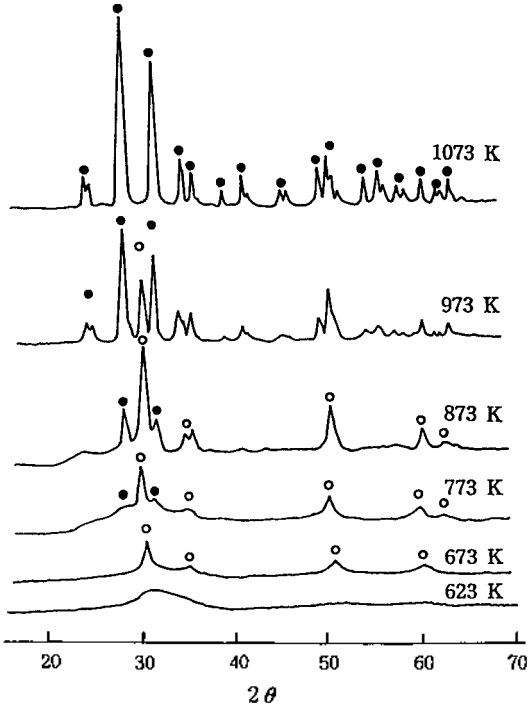

Figure 2. X-ray diffraction patterns of 2-V_2O_5-ZrO_2 calcined at different temperature for 1.5 hr. ○ : tetragonal phase ZrO_2, ● : monoclinic phase ZrO_2.

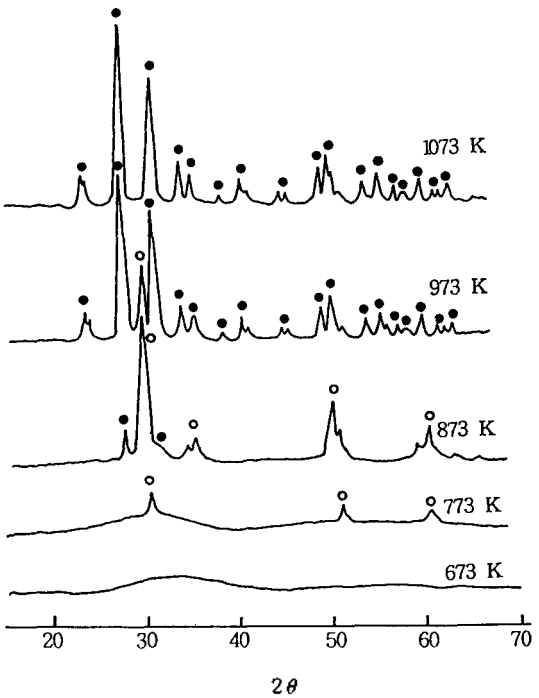

Figure 3. X-ray diffraction patterns of 9-V_2O_5-ZrO_2 calcined at different temperature for 1.5 hr. ○ : tetragonal phase ZrO_2, ● : monoclinic phase ZrO_2.

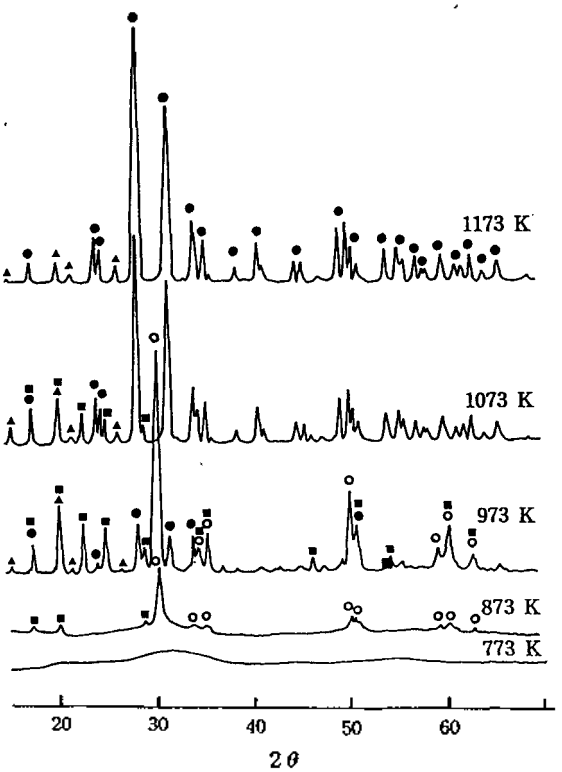

Figure 4. X-ray diffraction patterns of 15-V_2O_5-ZrO_2 calcined at different temperature for 1.5 hr. ○ : tetragonal phase ZrO_2, ● : monoclinic phase ZrO_2, △ : orthorhombic phase V_2O_5, ■ : cubic phase ZrV_2O_7.

to 573 K, with a two-phase mixture of the tetragonal and monoclinic forms at 623-873 K, and a monoclinic phase at 973 K. Three crystal structures of ZrO_2, tetragonal, monoclinic and cubic phases have been reported.[18,19]

However, in the case of supported vanadium oxide catalysts the crystalline structures of samples were different from that of ZrO_2 support. For the 2-V_2O_5/ZrO_2, as shown in Figure 2, ZrO_2 was amorphous up to 623 K. In other words, the transition temperature from amorphous to tetragonal phase was higher by 50 K than that of pure ZrO_2. X-ray diffraction data indicated a tetragonal phase of ZrO_2 at 673-773 K, a two-phase mixture of the tetragonal and monoclinic ZrO_2 forms at 873-973 K, and monoclinic ZrO_2 form at 1073 K. It is assumed that the interaction between vanadium oxide and ZrO_2 hinders the transition of ZrO_2 from amorphous to tetragonal phase.[20] The presence of vanadium strongly influences the development of textural properties with temperature in comparison with pure ZrO_2. Moreover, for the sample of 5 and 9-V_2O_5/ZrO_2, the transition temperature from amorphous to tetragonal phase was higher by 100 K and 150 K than that of pure ZrO_2, respectively. That is, the more the content of vanadium, the higher the transition temperature up to 9 mol%. For the samples above 9 mol%, however, the transition temperature did not increase more successively. These results are in agreement with those of DSC described below. 5-V_2O_5/ZrO_2 was amorphous to X-ray diffraction up to 673 K, with a tetragonal phase of ZrO_2 at 773 K, a two-phase mixture of the tetragonal and monoclinic forms at 873-973 K, and a monoclinic phase at 1073 K. As shown in Figure 3, 9-V_2O_5/ZrO_2 was amorphous to X-ray diffraction up to 773 K, with a tetragonal phase of ZrO_2 at 873 K and a monoclinic form at 973-1073 K. No phases of vanadium oxide were observed up to 9 mol% at any calcination temperatures below 1073 K, indicating a good dispersion of vanadium oxide on the surface of ZrO_2 support due to the interaction between them. These results are in good agreement with those of ^{51}V NMR described below.

As shown in Figure 4, however, for 15-V_2O_5/ZrO_2 cubic phase of ZrV_2O_7 phase were observed only in the samples calcined at 873 K, and the diffraction patterns at 973 K may point to a coexisting crystalline V_2O_5 phase. At 1073 K of calcination temperature the peak intensities of ZrV_2O_7 decreased to some extent, resulting from thermal decomposition of the ZrV_2O_7 into zirconia and vanadia.[21] Consequently, for sample calcined at 1173 K ZrV_2O_7 phase disappeared due to the complete decomposition of ZrV_2O_7, remaining only V_2O_5 phase and monoclinic phase of ZrO_2. These results are in agreement with those of ^{51}V solid-state NMR described below. In view of NMR (Figure 6), for high V_2O_5 loading samples, 15-V_2O_5/ZrO_2 and 20-V_2O_5/ZrO_2 calcined at 673 K the crystalline of V_2O_5 is observed clearly. However, as shown in Figure 4, the crystalline V_2O_5 on X-ray diffraction pattern is not found at 673 K of calcination temperature. This indicates that for samples calcined at 673 K the V_2O_5 crystallites formed are less than 4 nm in size, that is, beyond the detection capability of the XRD technique.

In X-ray diffraction pattern, it was shown that the structure of V_2O_5/ZrO_2 was different depending on the calcined temperature. To examine the thermal properties of precusors of samples more clearly, their thermal analysis was carried out and illustrated in Figure 5. For pure ZrO_2, the DSC curve

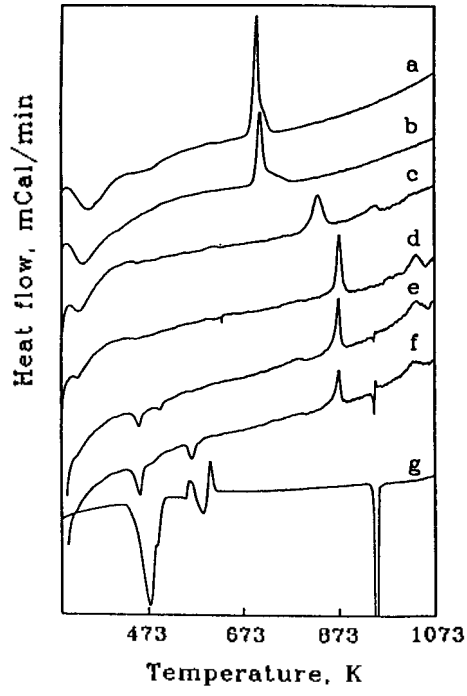

Figure 5. DSC curves of precursors of catalysts: (a) ZrO_2, (b) 1-V_2O_5/ZrO_2, (c) 5-V_2O_5/ZrO_2, (d) 9-V_2O_5/ZrO_2, (e) 15-V_2O_5/ZrO_2, (f) 20-V_2O_5/ZrO_2, and (g) NH_4VO_3.

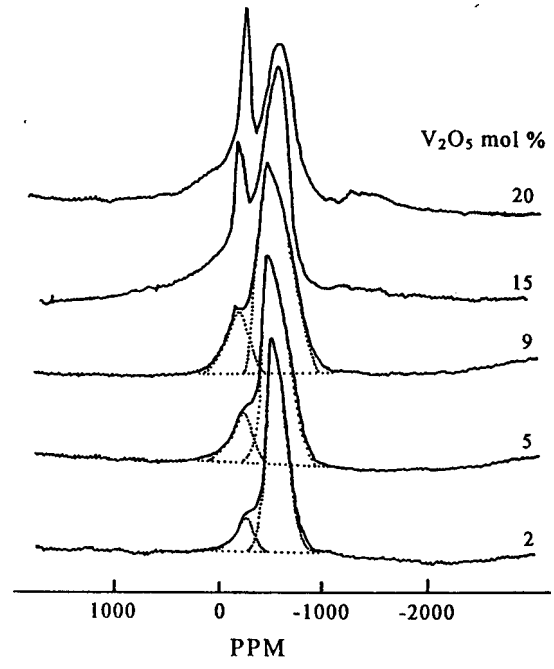

Figure 6. Solid-state ^{51}V NMR spectra of V_2O_5/ZrO_2 catalysts calcined at 673 K.

show a broad endothermic peak below 453 K due to water elimination, and a sharp and endothermic peak at 702 K due to the ZrO_2 crystallization.[22] In the case of V_2O_5/ZrO_2, two additional endothermic peaks appeared at about 454 and 563 K due to the revolution of NH_3 and H_2O decomposed from NH_4VO_3. Also, it is considered that an endothermic peak at 947 K is responsible for the melting of V_2O_5 and an exothermic peak around 989 K is due to the formation of ZrV_2O_7 crystalline described in X-ray diffraction patterns. However, it is of interest to see the influence of vanadium oxide on the phase transition of ZrO_2 from amorphous to tetragonal phase. As Figure 5 shows, the exothermic peak due to the phase transition appears at 702 K for pure ZrO_2, while for V_2O_5/ZrO_2 samples it is shifted to higher temperatures. The shift increases with increasing vanadium oxide content up to 9 mol% of V_2O_5. Consequently, the exothermic peaks appear at 710.1 K for 1-V_2O_5/ZrO_2, 830.7 K for 5-V_2O_5/ZrO_2 and 874.6 K for 9-V_2O_5/ZrO_2.

For the samples above 9 mol% of V_2O_5, however, the shift of transition temperature did not occur more successively, resulting in agreement with those of X-ray diffraction patterns described above. For the samples above 9 mol%, no more shift of transition temperature means that the content of vanadium oxide exceeding 9 mol% does not interact with the surface of zirconia. Moreover, as shown in Figure 5, the results that the endothermic peaks at 947 K due to the melting of V_2O_5 are not observed for samples containing low content of V_2O_5 up to 9 mol% support the above discussion more absolutely. That is, it is clear that the interaction between V_2O_5 forming monolayer on the surface of ZrO_2 and zirconia prevents V_2O_5 from melting and then only the amount of V_2O_5 exceeding 9 mol% melts easily.

On zirconia the V_2O_5 may be present as a monomolecular dispersion, covering most of the available surface.[23] The surface area of 9-V_2O_5/ZrO_2 calcined at 673 K is 150.0 m^2/g which is mainly contributed by ZrO_2, because V_2O_5 plays a role to protect catalyst from sintering. So, we can calculate the area of one V_2O_5 molecule occupying the surface of ZrO_2, resulting in 2.3 molecules nm^{-2}. This result is very similar with 2.4 molecules nm^{-2} reported by Hatayama *et al.*[24] In view of results of XRD, DSC, and surface area of V_2O_5, it is concluded that the content of V_2O_5 forming complete V_2O_5 monolayer on the surface of zirconia below transition temperature of ZrO_2 is 9 mol%. It is relavent that the strong interaction between vanadium oxide and zirconia delays the transition of ZrO_2 from amorphous to tetragonal phase.

Solid state NMR methods represent a novel and promising approach to vanadium oxide catalytic materials. The solid state ^{51}V NMR spectra of V_2O_5/ZrO_2 catalysts calcined at 673 K are shown in Figure 6. There are three types of signals in the spectra of catalysts with varying intensities depending on V_2O_5 content. At the low loadings up to 9 mol% V_2O_5 a shoulder at about -300 ppm and the intense peak at -550-650 ppm are observed. The former is assigned to the surface vanadium-oxygen structures surrounded by a distorted octahedron of oxygen atoms, while the latter is attributed to the tetrahedral vanadium-oxygen structures.[25,26]

However, the surface vanadium oxide structure is remarkably dependent on the metal oxide support material. Vanadium oxide on TiO_2 (anatase) displays the highest tendency to be 6-coordinated at low surface coverages, while in the case of γ-Al_2O_3 a tetrahedral surface vanadium species is the favored.[25] As shown in Figure 6, at low vanadium loading on ZrO_2 a tetrahedral vanadium species is exclusively dominant compared with a octahedral species. In general, it is known that low surface coverages favor a tetrahedral

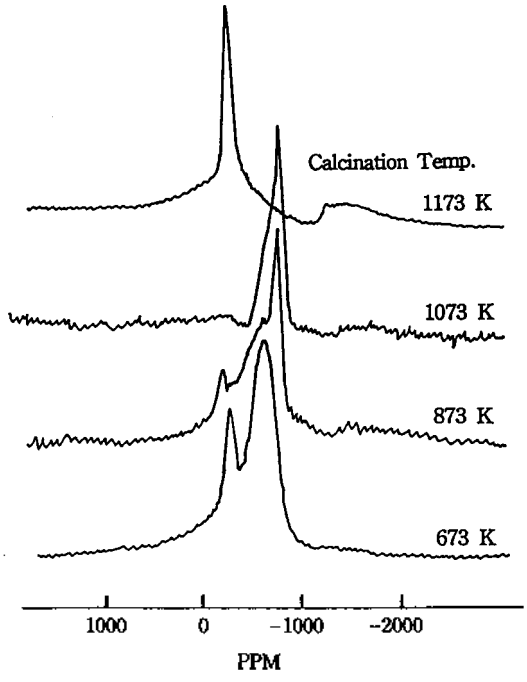

Figure 7. Solid-state ^{51}V NMR spectra of 15-V_2O_5/ZrO_2 catalysts calcined at different temperature.

coordination of vanadium oxide, while at higher surface coverages vanadium oxide becomes increasingly octahedral-coordinated.

The relative NMR signal intensities have been analyzed by appropriate curve fitting as shown in Figure 6. For 2-V_2O_5/ZrO_2 the peak area under the vanadium signal was 86.5%, while that of octahedral species was estimated to be 13.5%. For 5-V_2O_5/ZrO_2 and 9-V_2O_5/ZrO_2 the percentage of the octahedral NMR peak areas was estimated to be 17.6% and 21.7 %, respectively. Namely the relative amount of octahedral vanadium species increased with increasing vanadium loading. This finding agrees with earlier results of other workers.[25,26] Increasing the V_2O_5 content on the ZrO_2 surface changes the shape of the spectrum to a rather intense and sharp peak at about −300 ppm and a broad low-intensity peak at about −1400 ppm, which are due to the crystalline V_2O_5 of square pyramid coordinaton.[25]

The spectra of 15-V_2O_5/ZrO_2 calcined at various temperatures are shown in Figure 7. The shape of the spectrum is very different depending on the calcination temperature. For sample calcined at 673 K, a sharp peak at −300 ppm due to the crystalline V_2O_5 and an intense peak at −613 ppm attributable to V atoms in tetrahedral environment are observed. However, for sample calcined at 873 K, in addition to the above two peaks a sharp peak at −800 ppm due to crystalline ZrV_2O_7 appeared, indicating the formation of a new compound from V_2O_5 and ZrO_2 at high calcination temperature. As shown in Figure 4, for samples calcined at 873-1073 K X-ray diffraction patterns of ZrV_2O_7 was observed. Roozeboom *et al.* reported the formation of ZrV_2O_7 from V_2O_5 and ZrO_2 at 873 K of calcination temperature.[21,23] At 1073 K of calcination temperature only a peak at −802 ppm due to ZrV_2O_7 phase appeared, saying that most of V_2O_5 on the surface of ZrO_2 was consumed to form ZrV_2O_7 compound. However, at 1173 K of calcination temperature we can observe only a sharp peak of crystalline V_2O_5 at −294 ppm, indicating the decomposition of ZrV_2O_7. These results are in good agreement with those of X-ray diffraction patterns in Figure 4. In X-ray diffraction pattern of 15-V_2O_5/ZrO_2 calcined at 1173 K we can observe the presence of crystalline V_2O_5 and monoclinic ZrO_2 produced through the complete decomposition of ZrV_2O_7.

Conclusions

The interaction between vanadium oxide and zirconia influences the physicochemical properties of prepared catalysts with calcination temperature. The presence of vanadium oxide delays the phase transitions of zirconia from amorphous to tetragonal in proportion to the vanadium oxide content up to 9 mol%. On the basis of results of DSC, XRD and ^{51}V solid-state NMR, the V_2O_5 content forming complete monolayer on the surface of ZrO_2 was estimated to be 9 mol%. Below transition temperature of ZrO_2 from amorphous to tetragonal phase the ZrO_2 stabilizes supported vanadium oxide and vanadium oxide up to 9 mol% is well dispersed on the surface of ZrO_2. However, V_2O_5 loading exceeding the formation of complete monolayer (9 mol%) on the surface of ZrO_2 was well crystallized and observed in the spectra ^{51}V solid-state NMR.

Acknowledgment. This paper was supported by the Research Center for Catalytic Technology of the Korea Science and Engineering Foundation.

References

1. Nakagawa, Y.; Ono, T.; Miyata, H.; Kubokawa, Y. *J. Chem. Soc., Faraday Trans. 1* **1983**, *79*, 2929.
2. Miyata, H.; Kohno, M.; Ono, T.; Ohno, T.; Hatayama, F. *J. Chem. Soc. Faraday Trans. 1* **1989**, *85*, 3663.
3. Gellings, P. J., in *Spec. Per. Rep.* "Catalysis" (G. C. Bond and G. Webb, Eds.) Royal Society of Chemistry, London, **1985**, *7*, 105.
4. Bosch, H.; Janssen, F. *Catal. Today* **1988**, *2*, 369.
5. Forzatti, P.; Tronoconi, E.; Busca, G.; Titarellp, P. *Catal. Today* **1987**, *1*, 209.
6. Busca, G.; Elmi, A. S.; Forzatti, P. *J. Phys. Chem.* **1987**, *91*, 5263.
7. Elmi, A. S.; Tronoconi, E.; Cristiani, C.; Martin, J. P. G.; Forzatti, P. *Ind. Eng. Chem. Res.* **1989**, *28*, 387.
8 Miyata, H.; Fujii, K.; Ono, T.; Kubokawa, Y.; Ohno, T.; Hatayama, F. *J. Chem. Soc., Faraday Trans. 1* **1987**, *83*, 675.
9. Cavani, F.; Centi, G.; Foresti, E.; Trifiro, F. *J. Chem. Soc., Faraday Trans. 1* **1988**, *84*, 237.
10. Hayata, F.; Ohno, T.; Maruoka, T.; Miyata, H. *J. Chem. Soc., Faraday Trans.* **1991**, *87*, 2629.
11. Arco, M. del, Holgado, M. J.; Martin, C.; Rives, V. *Langmiur* **1990**, *6*, 801.
12. Centi, G.; Pinelli, D.; Trifiro, F.; Ghoussoub, D.; Guelton, M.; Gengembre, L. *J. Catal.* **1991**, *130*, 238.
13. Inomata, M.; Mori, K.; Miyamoto, A.; Murakami, Y. *J. Phys. Chem.* **1983**, *87*, 761.

14. Miyata, H.; Kohno, M.; Ono, T. *J. Mol. Catal.* **1990**, *63*, 181.
15. Scharf, U.; Schraml-Marth, M.; Wokaun, A.; Baiker, A. *J. Chem. Soc., Faraday Trans.* **1991**, *87*, 3299.
16. Miyata, H.; Kohno, M.; Ono, T.; Ohno, T.; Hatayama, F. *J. Mol. Catal.* **1990**, *63*, 181.
17. Hayashi, S.; Hayamizu, K. *Bull. Chem. Soc. Jpn.* **1990**, *63*, 961.
18. Torralvo, M. J.; Alario, M. A.; Soria, J. *J. Catal.* **1984**, *86*, 473.
19. Clearfield, A. *Inorg. Chem.* **1964**, *3*, 146.
20. Sohn, J. R.; Ryu. S. G. *Langmuir* **1993**, *9*, 126.
21. Roozeboom, F.; Mittelmeljer-Hazeleger, M. C.; Moulijn, J. A.; Medema, J.; de Beer, V. H. J.; Gellings, P. J. *J. Phys. Chem.* **1980**, *84*, 2783.
22. Livage, J.; Doi, K.; Mazieres, C. *J. Am. Ceram. Soc.* **1968**, *51*, 349.
23. Roozeboom, F.; Fransen, T.; Mars, D.; Gellings, P. J. Z. *Anorg. Allg. Chem.* **1979**, *449*, 25.
24. Hayata, F.; Ohno, T.; Maruoka, T.; Miyata, H. *J. Chem. Soc., Faraday Trans.* **1991**, *87*, 2629.
25. Eckert, H.; Wachs, I. E. *J. Phys. Chem.* **1989**, *93*, 6796.
26. Reddy, B. M.; Reddy, E. P.; Srinivas, S. T.; Mastikhim, V. M.; Nosov, N. V.; Lapina, O. B. *J. Phys. Chem.* **1992**, *96*, 7076.

Lipid Specificity for Membrane Oxidation Catalyzed by Cytochrome c : An EPR Study

Tongpil Min and Sanghwa Han*

Department of Biochemistry, Kangwon National University, Chunchon 200-701, Korea
Received January 8, 1996

Decay of the spin label attached to cytochrome *c* or to stearic acid has been measured by electron paramagnetic resonance (EPR) spectroscopy to monitor membrane oxidation induced by cytochrome *c*-membrane interaction. Binding of cytochrome *c* sequestered the acidic phospholipids and membrane oxidation was efficient in the order linoleic≫ oleic>stearic acid for a fatty acid chain in the acidic phospholipids. The spin label on cyt *c* was destroyed at pH 7 whereas that on stearic acid embedded in the membrane was destroyed at pH 4, presumably due to different modes of cyt *c*-membrane interaction depending on pH. Interestingly, cyt *c* also interacts with phosphatidylethanolamine, an electrically neutral phospholipid, to cause rapid membrane oxidation. Both EPR and fluorescence measurements indicated that electrostatic interaction is at least partially responsible for the process.

Introduction

Cytochrome *c* (Cyt *c*) is a peripheral membrane protein in the intermembrane space of mitochondria. Being abundant in lysine residues, the protein carries a large positive charge at physiological pH. The inner mitochondrial membrane, on the other hand, is rich in cardiolipin (CL) which makes the membrane surface electrically negative. Therefore cyt *c* is expected to interact electrostatically with the inner membrane.[1] The consequences of the cyt *c*-membrane interaction include alteration in the heme coordination state,[2] partial unfolding of the polypetide,[3] and disruption of the bilayer structure.[4,5] It is not clear if such interaction plays a role *in vivo*. Gupte and Hackenbrock[6] argued that ionic strength in the intermembrane space is too high for cyt *c* to interact electrostatically with the membrane. Recently, however, the same group[7] reported that a fraction of cyt *c* interacts with the membrane even under the condition of high ionic strength. Rytömaa and Kinnunen[8] suggested that the interaction of cyt *c* and acidic membranes is not electrostatic in nature at low pH. In their model, the protonated phosphate group of a phospholipid forms a hydrogen bonding network with an arginine residue of cyt *c*. Therefore cyt *c* may well interact with the inner mitochondrial membrane under certain conditions.

Using spin-label EPR techniques,[9] we were able to distinguish spectroscopically different states of bound cyt *c* at pH 7 and 4. During the experiments, however, we found that the EPR intensity of the spin label attached to cysteine-102 decayed rapidly when cyt *c* was allowed to interact aerobically with a membrane that contained acidic phospholipids. A similar observation was made some 20 years ago by Brown and Wüthrich,[10] who used horse heart cyt *c* with a spin label attached to methionine-65. Kinetic properties are rather complicated but a few things about the phenomenon are obvious from their work: electrostatic interaction between positively charged cyt *c* and a negatively charged membrane is required; both a lipid oxidation product, if pre-existent, and oxygen are involved; and the spin label on cyt *c* as well as that inside the membrane is destroyed. The lipid oxidation product, a reactive species that destroyed the spin labels, may be lipid hydroperoxides which undergo homolytic scission by the heme. In addition, Goñi and coworkers[11,12] included the binding of cyt *c* to the membrane and the presence of cyt *c* in the oxidized state as the requirements for the membrane oxidation. Other heme proteins are also known to